PFC/JA-93-10 REV

Quench in Superconducting Magnets, Part I: Model and Numerical Implementation

A. Shajii and J.P. Freidberg

January, 1994

Plasma Fusion Center
Massachusetts Institute of Technology
Cambridge, MA 02139 USA

Submitted for publication in: **Journal of Applied Physics**

This work was supported by the US Department of Energy through the Idaho National Engineering Laboratory under contract C88-110982-TKP-154-87. Reproduction, translation, publication, use, and disposal, in whole or in part, by or for the US Government is permitted.

Table of Contents

Abstract

A new simple, self consistent theoretical model is presented that describes the phenomena of quench propagation in Cable In Conduit superconducting magnets. The model circumvents many of the difficulties associated with obtaining numerical solutions in more general existing models. Specifically, a factor of 30-50 is gained in CPU time over the general, explicit time dependent codes used to study typical quench events. The corresponding numerical implementation of the new model is described and the numerical results are shown to agree very well with those of the more general models, as well as with experiment al data.

1. Introduction

Superconducting magnets have many applications in large government and industrial projects. They are particularly useful in situations where high magnetic fields are required but economic or technological considerations limit the total steady state electrical power available. Such projects include the toroidal and poloidal field coils for magnetic fusion experiments, the detector magnets for high energy particle accelerators, and the coils for magnetically levitated public transportation (MAGLEV). Because of the high construction costs involved, magnet protection in the event of faults is one of the crucial design elements. One of the most serious faults is that of quenching, a situation wherein a local section of the magnet, because of some local heat perturbation, returns to its normal state. If the perturbation is large enough, neighboring sections of the magnet are subsequently quenched because of heat convection by the coolant. If the quench is not detected quickly enough, the normal zone propagates along the entire length of the coil, quenching the entire magnet. Late detection of quench invariably causes irreversible damage to the magnet. The purpose of this paper is to present a new compact model that describes the process of quench in Cable In Conduit Superconducting Magnets, and a corresponding, highly efficient, numerical implementation. In the accompanying paper, Part II, the new model is further simplified by means of several additional approximations valid for many superconducting magnets. This leads to an ultra-fast numerical procedure and an analytic solution.

Cable In Conduit Conductors (CICC) consist of a superconducting cable surrounded by supercritical helium [1]. The helium is used to cool the superconductor during steady state operation. The system of helium and cable is surrounded by a conduit generally made of stainless steel. Figure 1 shows a schematic diagram of the cross section of a CICC; typically the conduit has an overall diameter of the order of a few centimeters, while the conductor has a length of a few hundred meters. The superconducting cable consists of a large number of strands (20-500) that enhance the heat transfer between the cable and the helium. These strands are made of a superconducting alloy embedded in a copper matrix. The alloy remains in its superconducting state when its temperature T lies below a critical

value T_{cr}. Above T_{cr}, the alloy has a very high electrical resistivity. The copper matrix is used to carry the current in the event that the temperature in a section of the cable is accidentally raised above T_{cr}. In such a situation the current flows preferentially through the copper matrix which acts as a parallel resistor to the high resistivity, "quenched" section of the superconducting alloy. This allows for a large reduction of ohmic dissipation that would otherwise be present in the superconducting alloy. Even so, because of the high current flowing in the cable, it often takes only a few seconds for the quenched section of the cable to rise from its cryogenic temperature $T \approx 5$K and pressure $p \approx 5$ atm to values of $T \approx 250$K and $p \approx 25$ atm. Past this point, irreversible damage to the magnet can occur (e.g. thermal stresses become larger than the shear strength of the insulating material).

The problem of quench propagation in CICC magnets has been known and qualitatively understood for many years [1,2,3]. Several excellent, sophisticated numerical codes have been developed to model quench events with sufficient accuracy for engineering design purposes [4,5]. These codes are fairly general in their engineering and physics content. Consequently, they have the advantage of being able to investigate not only quench propagation, but other phenomena such as startup, stability, etc. However, because of their generality they often require large CPU time/run (typically several hours of CRAY time for a 3 second quench simulation), a disadvantage from the engineering design point of view. In fact this has been the primary motivation for the present work, and has led to a number of advances in the modelling of quench propagation. The main new contributions are summarized below.

a. A compact model has been developed that focuses solely on the problem of quench. The model is a simpler form of that used in existing general codes, and is obtained by exploiting the high heat transfer between helium and cable and the fact that the flow velocities are highly subsonic.

b. Because of the simplicity of the model, we have been able to develop a fast, efficient, and robust numerical code. It is fully implicit in time, automatically remeshes the grid to follow the quench front, and requires one to two orders of magnitude less CPU time than the existing codes. (After completion of this paper, we learned that

L. Bottura was finishing development of an implicit version [6] of his general explicit magnet design code. This new code should significantly reduce the CPU time and in the near future we plan to compare it in detail with the code developed here.)

c. The speed and accuracy of the code is verified by three specific applications. First, a comparison is made with one of the existing general codes on a 2 second simulation of one of the ITER coils for the next generation fusion reactor [7]. Second, to demonstrate speed, a realistic 50 second quench simulation is performed. Third, a detailed comparison is made with the experimental results of Ando et al. [8].

The remainder of the paper is organized in four sections. In section 2 we present the general model used in existing codes to describe quench events in a CICC, and discuss the computational difficulties involved in solving these equations. In section 3 we consider simplifications of the general model focussing solely on the problem of quench. These simplifications circumvent most of the difficulties of modelling quench. The numerical procedure used to solve the simplified quench model is discussed in section 4. The simplified model is shown to be quite accurate in describing quench propagation, while saving significantly in computational cost. Finally in section 5 we present comparisons of results from the simplified model with those of the general model, as well as with experimental data.

2. General Model

In this section we describe a general superconducting magnet model which serves as the basic core for most existing multi-purpose CICC simulators [4,5]. Once the general model is established, several well justified simplifications are introduced by focusing solely on the problem of quench. This ultimately leads to a more compact and computationally efficient model.

To begin consider a CICC of length L, whose cross-sectional area is illustrated in Fig. 1. In the paper, subscripts c, h and w denote the conductor strands, the helium, and the conduit wall respectively. For simplicity of presentation the conduit is assumed to be surrounded by a perfect insulator implying that $\kappa_w \mathbf{n} \cdot \nabla T_w = 0$ on the conduit-insulator

interface. (This assumption is not required in the general multi-purpose models or the quench model described in this paper.) The cross sectional length scale of the CICC ($\approx$ 0.1 m) is always much smaller than its axial length ($\approx$ 100-1000 m). The large difference between axial and radial scale lengths provides strong justification for the use of a one dimensional model to describe the quench event. Below are given the appropriate one dimensional equations describing each component of the CICC.

The Conductor

Denote x as the axial length along the channel. The governing energy equation describing the thermal evolution of the conductor is

$$\rho_c C_c \frac{\partial T_c}{\partial t} = \frac{\partial}{\partial x}\left(\kappa_c \frac{\partial T_c}{\partial x}\right) - \frac{hP_c}{A_c}(T_c - T_h) + S(T_c, x, t) \tag{1}$$

Equation (1) is a heat diffusion equation for the total assembly of conductor strands, each strand assumed indistinguishable from all others. Here T_c is the conductor temperature, T_h is the helium temperature, ρ_c is the density, C_c is the specific heat, κ_c is the thermal conductivity, h is the heat transfer coefficient between the helium and the conductor, and A_c and P_c denote the combined cross-sectional area and wetted-perimeter of all the strands, respectively. The quantity S is the heat source existing in the conductor strands. This source is due to the joule heating that occurs in conductor regions where the temperature is above the critical temperature T_{cr}; that is, in regions where the conductor is normal. The source is given by

$$S_c(T_c, x, t) = \eta_c J^2 \, H(T_c) \tag{2}$$

where $J(t) = I(t)/A_{cu}$ is the current density in the copper, $I(t)$ is the prescribed current in the conductor, A_{cu} is the fractional area of A_c occupied by copper, $\eta_c(T_c, B)$ is the resistivity of copper (a strong function of the temperature), $B(x,t)$ is the magnetic field in the cable, and H is a Heaviside-like transition function from the normal to superconducting regions. $H(T_c)$ is illustrated in Fig. 2.

The Conduit Wall

The heat diffusion equation for the conduit wall is similar to Eq. (1) and is given by

$$\rho_w C_w \frac{\partial T_w}{\partial t} = \frac{\partial}{\partial x}\left(\kappa_w \frac{\partial T_w}{\partial x}\right) - \frac{hP_w}{A_w}(T_w - T_h) \tag{3}$$

where the thermal properties C_w and κ_w are functions of T_w. The quantities here are the obvious analogs to those in the conductor. All the existing codes, including the one described here, have a Joule heating source term on the right-hand side of Eq. (3). Often it is a good approximation to neglect this source term because of the high resistivity of the conduit wall. Here, for simplicity of presentation, we ignore the Joule heating term.

The Helium

The governing one dimensional equations describing the supercritical helium are that of mass, momentum and energy for a compressible gas, coupled with the equation of state;

$$\frac{\partial \rho_h}{\partial t} + \frac{\partial}{\partial x}(\rho_h v_h) = 0 \tag{4}$$

$$\rho_h \frac{\partial v_h}{\partial t} + \rho_h v_h \frac{\partial v_h}{\partial x} = -\frac{\partial p_h}{\partial x} - \frac{f \rho_h v_h |v_h|}{2 d_h} \tag{5}$$

$$\rho_h C_h \frac{\partial T_h}{\partial t} + \rho_h C_h v_h \frac{\partial T_h}{\partial x} + \rho_h C_\beta T_h \frac{\partial v_h}{\partial x} = \frac{hP_c}{A_h}(T_c - T_h) + \frac{hP_w}{A_h}(T_w - T_h) + \frac{f \rho_h |v_h| v_h^2}{2 d_h} \tag{6}$$

$$p_h = p_h(\rho_h, T_h) \tag{7}$$

Equations (4–6) evolve the fluid variables ρ_h, v_h, and T_h forward in time. The terms on the left-hand side of Eq. (5) describe the helium inertia, while the terms on the right-hand side represent the pressure gradient force and the friction force. The friction factor $f(\rho_h, T_h, v_h)$ models the turbulent friction between the solid components and the helium, and its functional dependence is assumed known from experimental measurements. The quantity d_h is the hydraulic diameter given by $4A_h/(P_w + P_c)$.

In Eq. (6) the terms on the left-hand side represent convection and compressibility. The first two terms on the right-hand side each involve the heat transfer coefficient $h(\rho_h, T_h, v_h)$, and account for the heat exchange between the helium and the solid components. This coefficient models the turbulent heat transfer taking place in the helium, and its value is assumed known from experimental correlations. The last term on the right-hand side of Eq. (6) represents the viscous (or frictional) heating of the helium. The quantity $C_h(\rho_h, T_h)$ is the specific heat of helium at constant volume, and $C_\beta(\rho_h, T_h)$ is defined as $C_\beta \equiv (1/\rho_h)\partial p_h(\rho_h, T_h)/\partial T_h = -\rho_h \partial \hat{S}(\rho_h, T_h)/\partial \rho_h$ where $\hat{S}$ is the entropy. Note that, thermal conduction in the helium has been neglected because its value is small compared to the convective terms.

Equations (1–7) describe the basic core of superconducting magnet models. Even though they are "only" one dimensional plus time, they are remarkably difficult to solve numerically for quench events, almost always requiring at least several hours of CRAY CPU time for such simulations. There are fundamental reasons for these difficulties as discussed below.

Consider the typical parameters characterizing a quench event in a large superconducting magnet. The time scale of interest is $\sim$ 1-10 sec, during which the quench region expands in length, starting from a few centimeters and reaching tens of meters in conductors of total length $\sim$ 100-1000 m. During this time the temperature of the system behind the quench front rises from cryogenic values of $\sim$ 5 K to near room temperature. Over this large temperature range several of the thermal properties of the system (C_c, C_w, η_c) increase by two to three orders of magnitude. This wide variation in parameters is the first of the computational difficulties.

Next, note that the dominant mechanism for propagating the quench front is convection of helium. The joule heated normal conductor heats the adjacent helium which is then convected away from the quench zone. The leading edge of the hot gas then heats conductor material still in its superconducting state ahead of the quench zone. This heat causes the conductor to go normal thus increasing the size of the quench zone. Essentially, the high temperature helium gas expands like a bubble against the cold helium ahead of

the quench front, thereby propagating the quench as it comes in contact with the cold conductor. Typically, the quench front may be several centimeters thick out of total conductor length of 100-1000 m. This narrow moving boundary layer is the second of the computational difficulties.

The third computational problem is a consequence of the fact that typical quench velocities are of the order 1-10 m/sec, which are much slower than the speed of sound c in the helium: $v_h/c \sim 0.01$. Thus, explicit time advance algorithms require a very large number of integration time steps ($\sim 10^4$), because of the Courant condition, significantly increasing the CPU time required.

The final difficulty is a result of the high heat transfer between the conductor and the helium arising from the large wetted-perimeter of the combined conductor strands. The net effect is that the thermal coupling terms $\sim h(T_c - T_h)/d_h$ in Eqs. (1) and (6) are characterized by $h/d_h \rightarrow \infty, T_c - T_h \rightarrow 0$, the classic situation of a mathematically stiff set of equations.

To summarize, the one dimensional core model presented here accurately describes a variety of phenomena in superconducting magnets including the important problem of quench propagation. However, numerical simulations using the full model are costly in terms of CPU time because of four problems, (1) large variations in the physical properties, (2) a very narrow moving boundary layer, (3) highly subsonic flow velocities, and (4) high heat transfer between the various CICC components.

3. Quench Model

The numerical difficulties just described can be greatly alleviated by focussing attention solely on the phenomena of quench. As a result, additional analytic approximations can be made which exploit the subsonic flow velocity and high heat transfer characteristic of quench in long CICC magnets. Furthermore, a sophisticated numerical solver developed by U. Ascher et al. [9] substantially reduces the difficulties associated with the moving boundary layer. This solver also has no great difficulty treating the large variation in the material properties.

In this section we describe the analytic approximations used to simplify the general model and show that the errors involved are indeed small for engineering purposes. The numerical issues are discussed in the following section.

High Heat Transfer Approximation

During the quench process in a CICC the heat transfer between the conductor and the helium is very high. This is due to the large wetted-perimeter of the conductor ($P_c \approx 1$ m) in contact with the helium, as well as the high value of the heat transfer coefficient $h \approx 1000$ W/m^2-K. For example, consider an assembly of conductor strands with $A_c \approx 10^{-4}$ m^2, $\rho_c C_c \approx 10^6$ W/m$^3 - K$, and a characteristic quench time scale $\tau \approx 5$ sec. Next, balance the time derivative term on the left-hand side of Eq. (1) with the heat transfer term on the right-hand side. We find $(T_h - T_c)/T_c \approx A_c \rho_c C_c / h P_c \tau \approx 0.02$. The high heat transfer forces the temperature difference between the conductor and the helium to be small. We exploit this fact by annihilating the heat transfer terms in Eqs. (1) and (6) (by adding appropriate linear combinations of the two equations) and then setting $T_c \approx T_h \equiv T$. This results in a single energy equation for T, the temperature of the conductor and the helium. We have thus eliminated mathematically stiff terms from the system.

A related problem associated with mathematical stiffness concerns the conduit wall. Its thermal conductivity is generally small. Typically, $\kappa_w / \kappa_c \approx 10^{-3} \ll 1$, which justifies neglecting the conduction term in the energy equation for the conduit wall. Doing so eliminates another mathematically stiff term from the system.

Note that in general the heat transfer between the helium and the conduit is not as good as for the helium and the conductor since $P_w \ll P_c$. The implication is that the conduit temperature can lag behind the helium temperature by a finite amount. Hence, it is *not* a good approximation to set $T_w \approx T_h$ as was done for the conductor. It is for this reason that the quench model maintains two temperatures T and T_w.

The Subsonic Flow Approximation

The helium flow characteristics in the CICC are dominated by the friction between the cable strands and the helium. The friction force is quite high due to the small hydraulic diameter of the channel (typically $d_h \approx 10^{-3}$ m), and in the momentum equation is balanced primarily by the pressure gradient force. In other words, the helium inertia $\rho dv/dt$ is small compared to either of the terms on the right-hand side of Eq. (5). As an example consider a helium density of 100 kg/m^3, $v \approx 5$ m/sec, $\tau \approx 5$ sec, $L \approx 100$ m and a pressure drop of $\Delta p \approx 10$ atm. Comparing terms we have $\rho v L/\Delta p\, \tau \sim 10^{-2}$. On this basis, the helium inertia is neglected in the momentum equation. In terms of wave propagation, the large friction and corresponding subsonic flow velocities cause sound waves to be highly damped in these channels.

Neglect of the helium inertia allows us to eliminate the shortest time scale from the problem (i.e., sound wave propagation time scale). Thus, the quench event can be followed on the helium velocity time scale, which is approximately two orders of magnitude longer.

The Quench Model

In view of the above simplifications, the final quench model reduces to

$$\frac{\partial \rho}{\partial t} + \frac{\partial}{\partial x}(\rho v) = 0 \tag{8}$$

$$\frac{\partial p}{\partial x} = -\frac{f \rho v |v|}{2 d_h} \tag{9}$$

$$\rho \hat{C}_t \frac{\partial T}{\partial t} + \rho \hat{C}_h v \frac{\partial T}{\partial x} + \rho \hat{C}_\beta T \frac{\partial v}{\partial x} = \frac{\partial}{\partial x}\left(\kappa \frac{\partial T}{\partial x}\right) + S(T,x,t) + \frac{h P_w}{A_c}(T_w - T) + \frac{A_h}{A_c}\,\frac{f \rho |v| v^2}{2 d_h} \tag{10}$$

$$p = p(\rho, T) \tag{11}$$

$$\rho_w C_w \frac{\partial T_w}{\partial t} = \frac{h P_w}{A_w}(T - T_w) \tag{12}$$

where $\hat{C}_h = (A_h/A_c)C_h, \hat{C}_\beta = (A_h/A_c)C_\beta$, $\hat{C}_t = \hat{C}_h + (\rho_c/\rho)C_c$, $\kappa = \kappa_c$ and $S(T,x,t)$ is given by Eq. (2). For convenience, the subscript h has been suppressed from ρ_h, T_h, and v_h. Equations (8-12) represent the desired, simplified, quench model, hereafter referred to as "Quencher."

4. Numerical Solution and Boundary Conditions

In this section we describe the numerical procedure and corresponding boundary conditions used to solve Quencher. A short discussion is also presented of the evaluation of the various material properties appearing in the model.

Numerical Procedure

Quencher is a set of nonlinear, coupled one dimensional plus time partial differential equations. After testing several possible numerical methods, we selected the procedure described below because of its speed and robustness. In essence, the method utilizes a fully implicit time advance algorithm which transforms the model into a set of ordinary differential equations at each time step. These ODE's are then solved by a global collocation procedure [9].

The time advance is accomplished by a standard, second order accurate algorithm as follows. Assume all quantities are known at times t and $t - \Delta t$. To evaluate the time derivative of any quantity Q at the new time $t + \Delta t$, we approximate

$$\left(\frac{\partial Q}{\partial t}\right)_{t+\Delta t} \approx L_2 Q \equiv \frac{1}{2\Delta t}\left[3Q(t+\Delta t, x) - 4Q(t,x) + Q(t-\Delta t, x)\right] \tag{13}$$

This is substituted into the quench model. All the variables and coefficients in the non-time derivative terms are evaluated at $t + \Delta t$; that is, the time advance is purely implicit. After defining a new variable $q \equiv -\kappa(T)\partial T/\partial x$, we can rewrite the quench model as a set of first order ordinary differential equations of the form

$$\frac{d\mathbf{u}}{dx} = \mathbf{F}(x, \mathbf{u}) \tag{14}$$

where the vector $\mathbf{u}$ is given by

$$\mathbf{u} = \begin{bmatrix} \rho \\ v \\ T \\ q \end{bmatrix} \tag{15}$$

and $\mathbf{F}$ is given as

$$F_1 = -\frac{1}{C_\alpha T}\left(\frac{f\rho|v|v}{2d_h} - \frac{\rho C_\beta q}{\kappa}\right) \tag{16}$$

$$F_2 = -\frac{1}{\rho}(L_2\rho + vF_1) \tag{17}$$

$$F_3 = -\frac{q}{\kappa} \tag{18}$$

$$F_4 = S(T) - S_w - \rho\hat{C}_t L_2 T + \frac{\hat{C}_h \rho v q}{\kappa} - \hat{C}_\beta \rho T F_2 + \frac{A_h}{A_c}\frac{f\rho|v|v^2}{2d_h} \tag{19}$$

All terms have been previously defined except C_α and S_w. The quantity C_α is defined as $C_\alpha \equiv (1/T)\partial p(\rho,T)/\partial\rho$. The term S_w represents the coupling of the conductor/helium with the conduit wall. It is found by explicitly solving Eq. (12) using the time advance algorithm described above, evaluating the material properties at the previous time step. Thus,

$$T_w(t+\Delta t) = \frac{T(t+\Delta t) + \epsilon[4T_w(t) - T_w(t-\Delta t)]}{1+3\epsilon} \tag{20}$$

where $\epsilon = (A_w/hP_w)(\rho_w C_w/2\Delta t)$ is evaluated at t. The coupling term then becomes

$$S_w(t+\Delta t) \equiv \frac{hP_w}{A_c}(T - T_w) = \frac{hP_w}{A_c}\,\epsilon(t)\left[\frac{3T(t+\Delta t) - 4T_w(t) + T_w(t-\Delta t)}{1+3\epsilon(t)}\right]. \tag{21}$$

Note, as $hP_w/A_w \to \infty$, then $\epsilon \to 0$ and $T_w \to T$ implying that $S_w \to (A_w/A_c)\rho_w C_w L_2 T$. As expected, in this limit S_w just adds a wall contribution to the combined heat capacity $\hat{C}_t$.

Equation (14) represents the basic set of equations to be solved at each time step. The numerical procedure in Quencher makes use of a sophisticated collocation procedure developed by U. Ascher et al. [9]. This package has the distinct advantage of rapidly and automatically remeshing the problem at every time step in accordance with the motion of

the quench front. As an example, a typical mesh might contain 150-200 points with the narrowest spacing corresponding to 1 cm out of a total simulation length of 1000 m. The mesh redistribution is vital to achieve a high computational efficiency and an accurate solution to the problem. In addition, the collocation procedure has proven remarkably robust, converging over a wide class of applications using a wide range of time steps.

Boundary and Initial Conditions

As stated, the primary goal of Quencher is to simulate quench events in superconducting magnets. To accomplish this an appropriate set of initial and boundary conditions must be provided. The conditions chosen generate a quench by a three-step procedure. First, the system is initialized with profiles representing "standard steady state operation;" the entire magnet is superconducting and no external sources are present. Second, a high power pulse, localized in space and time, is applied to raise the corresponding local temperature above the critical temperature. Third, after the source is removed, the local quench just initiated is allowed to propagate along the coil. It is the detailed behavior of this propagation that is our primary interest.

The actual specification of the initial and boundary conditions requires some discussion since Quencher describes the behavior of a composite material (i.e. conductor plus helium). Thus standard conditions for a single material may be inappropriate. Even so, it is clear from the basic mathematical structure of the model that three initial conditions and four boundary conditions are required; the helium/conductor equations have a double set of parabolic characteristics while the wall equation is a simple initial-value problem.

Consider first the initial conditions. The simplest case corresponds to the situation where the helium is purely static. For such operation the initial conditions are given by

$$\rho(x,0) = \rho_0 = \text{ const.}$$

$$T(x,0) = T_w(x,0) = T_0 = \text{ const.} \tag{22}$$

where ρ_0 and T_0 are input parameters. As expected, the Quencher model then implies that $p = p(\rho_0, T_0) = \text{const}$ and $v = 0$ for steady state operation.

A more general case allows forced flow of the helium. For most situations of interest, the coils are sufficiently long so that the pressure, density, and temperature gradients are weak. The steady state equations can then be solved by simply allowing $\Delta t \rightarrow \infty$ in Eqs. (13–19). The code quickly converges to the steady state solution which then serves as the initial condition for the quench initiation.

Assume now that appropriate initial conditions have been specified. The next step is to add an external high power, short duration, spatially localized heat source (S_{ext}) to the energy equation in order to raise the conductor temperature above T_{cr}. In Quencher, S_{ext} has the form

$$S_{ext}(x,t) = S_0 \exp[-3(x - x_0)^2/L_q^2] \qquad 0 < t < t_1. \tag{23}$$

Equation (23) describes a Gaussian pulse, centered at $x = x_0$ of width $L_q\sqrt{3}$. The total power input is approximately equivalent to that of a rectangular pulse of amplitude S_0 and width L_q. For large coils, typically $S_0 \sim 10^8$ w/m^3. The source length $L_q \sim 0.1 - 1.0$ m out of a total length of $200 \sim 1000$ m indicating a strong spatial localization. The pulse duration $t_1 \sim 10^{-3}$ sec, which is much shorter than the characteristic quench time $\sim 1 - 10$ sec. For $t > t_1$ the external source is eliminated, and the local quench just initiated is allowed to evolve over the long quench time scale. This is the regime of primary interest.

In order to evolve the system from its initial state over both the initiation phase $0 < t < t_1$, and the quench phase $t_1 < t \lesssim 10$ sec, appropriate boundary conditions must be supplied. The boundary conditions are slightly subtle for two reasons. First, conditions must be provided that allow for both inlet and outlet flows, including a smooth transition from one to the other (e.g. when a quench induced pressure pulse forces helium out of the inlet channel). Second, the presence of the thermal conductivity requires an additional boundary condition since the order of the system has been raised by one. This condition, however, seems an extra one, with no natural way for its specification. These difficulties are resolved as follows.

To begin, we specify the pressure at both ends of the channel. These are standard

conditions, valid for both inlet and outlet flows. Consider now the effect of thermal conductivity. During a quench two narrow moving fronts propagate away in opposite directions from the heating source. Each front is actually a boundary layer whose width is determined by the thermal conductivity. If thermal conductivity is not included, discontinuities appear in the solution, making it more difficult to solve numerically.

Even so, either behind or ahead of the front, the thermal conductivity has a negligible effect. To see this, note that the ratio of thermal conduction to convection is given by $(\kappa T')'/(\rho_h \hat{C}_h v T') \sim \kappa/\rho_h \hat{C}_h v L$. Behind the quench front $\kappa \sim 1000$ W/m-K, $\rho_h \sim 10$ kg/m^3, $\hat{C}_h \sim 3000$ J/kg-K, $v \sim 1$ m/sec and $L \sim 10$ m indicating that $\kappa/\rho_h \hat{C}_h v L \sim 3 \times 10^{-3}$. Similarly, ahead of the quench front $\kappa \sim 1000$ W/m-K , $\rho_h \sim 100$ kg/m^3, $\hat{C}_h \sim 3000$ J/kg-K, $v \sim 5$ m/sec and $L \sim 100$ m giving $\kappa/\rho_h \hat{C}_h v L \sim 7 \times 10^{-6}$.

We see that what is required is a boundary condition that allows the thermal conductivity to play its role in the quench front, but does not introduce an undue artificial influence at either end. This goal is achieved by the nonstandard condition of setting $(\kappa T')' = 0$ at each end of the channel, which is clearly consistent with the idea that thermal conduction is unimportant ahead of the front. Other boundary conditions involving T or $\kappa T'$ directly, introduce spurious boundary layers at the ends. The condition $(\kappa T')' = 0$ allows both T and $\kappa T'$ to float freely, thereby assuming their natural values. It is also valid for both inlet and outlet flows, as the arguments about the smallness of heat conduction apply to both types of flow. Note also that the smallness of κ makes the equations mathematically stiff. However, the global nature of Ascher's collocation procedure has no difficulty whatsoever with this problem.

In summary, the boundary conditions used to initiate and evolve the quench, with either static or forced flow, are given by

$$p(0,t) = p_i(t) \tag{24a}$$

$$p(L,t) = p_o(t) \tag{24b}$$

$$\frac{\partial}{\partial x}(\kappa \frac{\partial T}{\partial x})\bigg|_0 = 0 \tag{24c}$$

$$\left.\frac{\partial}{\partial x}(\kappa\frac{\partial T}{\partial x})\right|_L = 0 \tag{24d}$$

This completes the mathematical specification of the Quencher model.

Material Properties

In order to obtain a numerical solution to the Quencher model, it is necessary to evaluate the material properties that appear as coefficients in the equations. This is more or less straightforward with the exception of the heat transfer coefficient as shown below.

To begin, note that the properties of helium including $p, \partial p/\partial\rho, \partial p/\partial T$, κ_h, μ_h, C_h and C_p, which are all functions of ρ and T, are available as library routines. Similarly, the basic properties of the cable and conduit wall $\kappa_c, \eta_c, C_c, C_w$, which are functions of T, are also readily available in library form. The properties of the cable actually model the composite copper-superconductor strands; that is

$$\begin{aligned} \rho_c C_c &= \frac{1}{A_c}\left[A_{cu}\rho_{cu}C_{cu} + A_{sc}\rho_{sc}C_{sc}\right] \\ \kappa_c &\approx \frac{A_{cu}}{A_c}\kappa_{cu} \\ \eta_c &\approx \frac{A_{cu}}{A_c}\eta_{cu} \end{aligned} \tag{25}$$

and $A_c = A_{cu} + A_{sc}$. In addition, the critical temperature of the superconductor $T_{cr} = T_{cr}(B, J)$ is known experimentally. The properties thus far discussed are accurate to within $\pm 10\%$.

The next quantity of interest is the Darcy friction factor f. Experimental observations [10,11] indicate that in the regime of interest f can be approximated by

$$f \approx k_f \frac{0.184}{R^{0.2}} \tag{26}$$

where $R = \rho v d_h/\mu_h$ is the Reynold's number and $\mu_h(\rho, T)$ is the helium viscosity. The quantity k_f is a constant whose value depends upon the roughness of the solid surface in

contact with the helium. For typical CICC channels $k_f \approx 3$. It is believed to be accurate to within $\pm 20\%$.

The final quantity of interest is the heat transfer coefficient h defined in terms of the Nusselt number N as follows

$$h \equiv \frac{\kappa_h N}{d_h}. \tag{27}$$

Here, $\kappa_h(\rho, T)$ is the thermal conductivity of helium. For typical flow velocities $v \sim 1 - 10$ m/sec, the Reynold's number is sufficiently high (i.e. $R > 10^4$) along most of the coil that the turbulent Nusselt number N_t would appear to be the appropriate choice for Eq. (27). The value of N_t most often used in CICC design is a modified form of the Dittus-Boelter coefficient given by [11,12]

$$N_t = 0.026\ R^{0.8}\ P^{0.4}\ \left(\frac{T}{T_w}\right)^{0.716} \tag{28}$$

where $P = \mu_h C_p / \kappa_h$ is the Prandtl number. Equation (28) is valid if $R \gtrsim 10^4$.

Somewhat surprisingly, Eq. (28) is often *not* valid behind the quench front where the rapid depletion of helium can lower the density by as much as two orders of magnitude. At these low densities the Reynold's number is typically $R \sim 500 - 3000$; that is, in the important region where joule heating takes place, the flow is essentially laminar, characterized by a Nusselt number [13]

$$N_\ell = 4. \tag{29}$$

In the so-called transition region between $2 \times 10^3 \lesssim R \lesssim 10^4$ there is a sparsity of data and the detailed behavior of the Nusselt number is not well known. The Quencher code uses a hybrid model for N to substitute into Eq. (27). It has the form

$$N = (N_\ell N_t)^{1/2} \left[\frac{N_\ell^{1/2} + N_t^{1/2}(R^2/R_\ell R_t)^{\nu/2}}{N_t^{1/2} + N_\ell^{1/2}(R^2/R_\ell R_t)^{\nu/2}}\right] \tag{30}$$

where $R_\ell = 2 \times 10^3$ and $R_t = 10^4$ are the transition Reynold's numbers. The quantity ν is an arbitrary parameter that sets the steepness of the transition from laminar to turbulent flow. A plot of N vs. R for various values of ν is shown in Fig. 3. Note that as $R \to 0$, then $N \to N_\ell$. Similarly as $R \to \infty$, then $N \to N_t$. These are the appropriate limits. In

practice most of the quantities of interest are insensitive to the value of ν. In Quencher the value of ν is chosen to be $\nu = 4$.

This completes the discussion of the material properties used in Quencher.

5. Discussion

In this section we compare the results of the Quencher model with those of other general purpose CICC computer codes, as well as experimental data. In particular, we (1) compare Quencher results with those of the more general code Saruman, (2) show that Quencher is sufficiently fast in terms of CPU time to simulate realistically long quench events, and (3) compare Quencher results with the detailed experimental results obtained by Ando et al. [8].

Comparison of Quencher and Saruman

To begin, consider the proposed design [7] of the Toroidal Field Coil of the International Thermonuclear Experimental Reactor (ITER). This conductor is of length 530 m, with $d_h = 1.6 \times 10^{-3}$ m, $A_h = 4.5 \times 10^{-4}$ m^2, $A_{cu} = 3.9 \times 10^{-4}$ m^2, $A_{sc} = 2.6 \times 10^{-4}$ m^2, $A_w = 2.6 \times 10^{-4}$ m^2, $P_w = 0.13$ m, and $I = 4.3 \times 10^4$ A. The current is kept constant for a period of 2 sec, after which it decays exponentially with a time constant of 20 sec. The conductor is in a uniform magnetic field of 13 T, and for simplicity of comparison with Saruman the heat transfer coefficient is taken to be a constant; $h = 500$ W/m$^2-$ K. Before the initiation of quench, the helium in the channel is stagnant at a temperature of 5 K and a pressure of 5 atm. Quench is initiated by depositing 1×10^5 W/m, at the center of the channel, over a 2 m length for a period of 0.01 sec. The temperature and density profiles as functions of x, at $t = 10$ sec from Quencher are shown in Figs. 4a and 4b, respectively. The temperature in the quench zone is increasing due to the joule heating. This tends to increase the pressure, giving rise to a flow of helium, thereby depleting the density in this region. In these figures we have plotted the actual mesh points used in the calculation at this particular time step. Note the distribution of mesh points along the length of the

conductor. The boundary layer at the location of the quench front, discussed in section 2, can be observed in these figures.

The computer code Saruman which is of the class of general codes discussed in section 2, is used to compare with Quencher. Saruman is a finite element code that solves the fluid equations described in section 2 using an explicit time advance algorithm [4]. We carry out the same 2 second quench simulation of the ITER coil as computed by Quencher. In Saruman we use a total of 800 elements with 600 placed within a 30 m length at the center of the channel for maximum resolution. The length of each element within the quench region is thus 5 cm; note that within the boundary layer the spacing between grid points used in Quencher is between 3 to 5 cm. Figures 5a and 5b show the comparison of the maximum conductor temperature and the maximum helium pressure, respectively, as functions of time. Since the problem is symmetric these maxima occur at the center of the channel. The length of the normal zone, $X_q(t)$, as a function of time is shown in Fig. 5c. The differences observed in these figures are indeed small and are believed to be due to the slightly different initial conditions used in the two models. In Saruman the external heat pulse used to initiate the quench is directly deposited in the conductor. In Quencher, this external heat is deposited in both the conductor and helium. Thus the amplitude of the external heat required to initiate the quench is slightly different in the two models. This difference gives rise to the constant offsets observed in Figs. 5a-c.

The velocity of helium at either end of the channel is presented in Fig. 4d. In Quencher the speed of sound time delay is not present; thus, helium expulsion from the channel occurs earlier than is physically possible. This early expulsion of helium, however, does not reduce the accuracy of the solution of the problem within the quench region as evidenced by Fig. 5a-c. In order to obtain the physical value of the helium velocity at the end of the channel, the results of Quencher are valid only after a time $t = L/2c$, where L is the length of the channel and c is the speed of sound in the helium (c is evaluated at the background ($t = 0$) pressure and temperature). For $t < L/2c$ the expulsion velocity is zero.

A Long Quench Simulation

The CPU time used by Saruman during the 2 second quench simulation presented in Fig. 5a-d, is approximately 10 hours on a CRAY-2 Supercomputer. Quencher requires approximately 50 minutes of CPU time on a VAX Station 4000/90. This saving in computing cost is essential in order to perform studies of quench for realistically long periods of time. In Fig. 6 we show the normal length as a function of time during a 50 second quench in the ITER conductor as computed by Quencher. The results represent the extension, from 2 to 50 seconds, of the quench event discussed above. After the current starts to decay, which is at $t = 2$ sec in this case, larger time steps can be used without losing accuracy in the solution. The CPU time used in the 50 second simulation is approximately 6 hours on the VAX 4000/90.

In several other cases where we have made detailed comparisons between Quencher and Saruman, the agreement has been equally good. We have found Quencher to be 30-50 times faster than Saruman in terms of the CPU time required to study quench events. One somewhat more difficult comparison occurs when the area of the conduit wall A_w becomes very small. In this regime a much larger number of elements in Saruman is required to achieve convergence. This causes Saruman to require prohibitively large CPU time. Even so, the results of Saruman appear to be converging to those of Quencher in the limit of small A_w.

Comparison of Quencher with Experiment

In order to compare the results of Quencher with experimental data we consider the clean and unambiguous measurements carried out by T. Ando et al. [8]. The CICC used in this experiment has a length 26 m, $A_{cu} = 1.02 \times 10^{-5}$ m^2, $A_{sc} = 3.4 \times 10^{-6}$ m^2, $A_w = 2.5 \times 10^{-5}$ m^2, $A_h = 1.4 \times 10^{-5}$ m^2, $d_h = 6.9 \times 10^{-4}$ m, and $P_w = 0.019$ m. The conductor is in a uniform magnetic field of 7 T. The results of the experiment are presented in the form of a plot of the normal length as a function of time, for various values of the conductor current. Before initiation of quench, the helium is stagnant at a temperature

of 4.5 K and a pressure of 10 atm. The ends of the channel are connected to pressure relief valves which maintain the helium pressure at 10 atm. Both in the experiment and Quencher the quench is initiated by depositing the external heat at the center of the conductor, over a 40 mm length for a period of 0.1 msec. In Quencher the amount of heat deposited to initiate the quench is 2.7×10^6 W/m (this corresponds to a total energy deposition of 2.7 J/cm.) This value is not explicitly given in the paper by Ando et al. [8]. It has been chosen to match the first data point for the case $I = 2$ kA and is then held fixed for all other values of I.

The comparison of Quencher results with the experimental data is presented in Fig. 7. The minimum and maximum values of the current used in the experiment are 1.5 and 2 kA, respectively. Note the large variation of the normal length with current at any given time; the dependence of normal length on current is in fact nearly exponential. Here, the heat transfer coefficient and the friction factor used in Quencher are given by the models presented in section 4. We have found the Quencher results presented in Fig. 7 to be nearly independent (≤ 1 %) of the value of ν used in Eq. (30), for $2 \leq \nu \leq 8$. Also, the dependence is very weak (≤ 15 %) on the value of k_f used in Eq. (26), for $1 \leq k_f \leq 5$. The agreement of the computational data and the experiment is very good and well within the uncertainties of the material properties of the various components.

6. Conclusion

The problem of quench propagation is of great importance for safety considerations in the design of superconducting magnets. By concentrating on the specific problem of quench, it has been possible to derive a simplified model that is highly accurate, but avoids most of the numerical difficulties found in more general models. An efficient numerical implementation of the simplified quench model (Quencher) has been presented and shown to be computationally cost efficient. In order to study the behavior of quench for longer periods of time, or to perform parametric studies on new conductor designs it is required to utilize a model such as Quencher because of the prohibitive amount of CPU time required

to solve the general models. The results of Quencher have been shown to agree well with those of more general models as well as experimental data.

Acknowledgments

The authors would like to thank the members of the Engineering Division at MIT's Plasma Fusion Center for many useful discussions during the course of the work. Several engineers are specifically acknowledged for their detailed and helpful suggestions: E. A. Chaniotakis, J. McCarrick, J. Minervini, D. B. Montgomery, R. Pillsbury, J. Schultz, and R. Thome.

This work was supported by the US Department of Energy under Grant C88-110982-TKP-154-87.

References

[1] Wilson, M. N., Superconducting Magnets, Oxford University Press, New York, 1983, pp. 306-309.

[2] Dresner, L., 11th Symposium on Fusion Engineering, Proceedings Vol. 2, IEEE, New York, 1986.

[3] Dresner, L., Cryogenics, Vol. 24, No. 6, 1984.

[4] Bottura, L., Zienkiewicz, O. C., Cryogenics, Vol. 32, No. 7, 1992.

[5] Wong, R. L., Program CICC Flow and Heat Transfer in Cable-In-Conduit Conductors – Equations & Verification, Lawrence Livermore National Laboratory Internal Report, UCID 21733, May 1989.

[6] Bottura, L., private communication, 1993.

[7] Rebut, P. H., IEEE/NPSS 15th Symposium on Fusion Engineering, Oct. 1993.

[8] Ando, T., Nishi, M., Kato, T., Yoshida, J., Itoh, N., Shimamoto, S., Advances in Cryogenic Engineering, Vol. 35, Plenum Press, New York, 1990.

[9] Ascher, U. M., Christiansen, J., Russell, R. D., ACM Transactions on Mathematical Software, Vol. 7, No. 2, 1981.

[10] Lue, J. W., Miller, J. R., Lottin, J. C., IEEE Trans. Magnet. Mag-15, 53 (1979).

[11] Van Sciver, S. W., Helium Cryogenics, Plenum Press, New York, 1986, pp. 243-244.

[12] Giarratano, P. J., Arp, V. D., Smith, R. V., Cryogenics, Vol. 11, 1971.

[13] Bird, R. B., Stewart, W. E., Lightfoot, E. N., Transport Phenomena, John Wiley & Sons, New York, 1960, pp. 404-406.

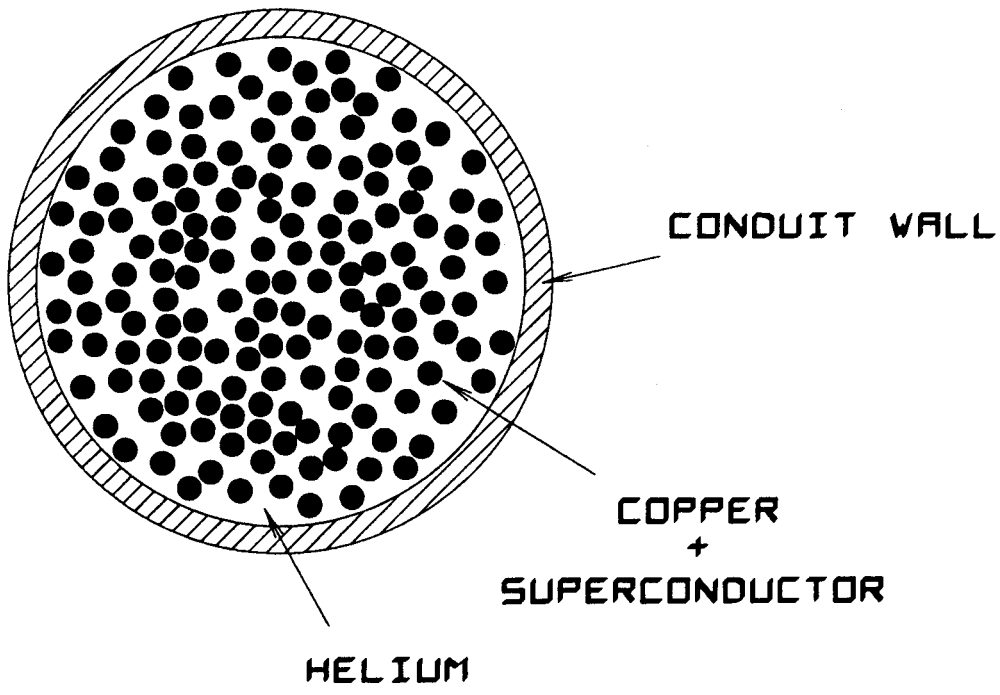

Figure 1: Schematic of the cross section of a CICC.

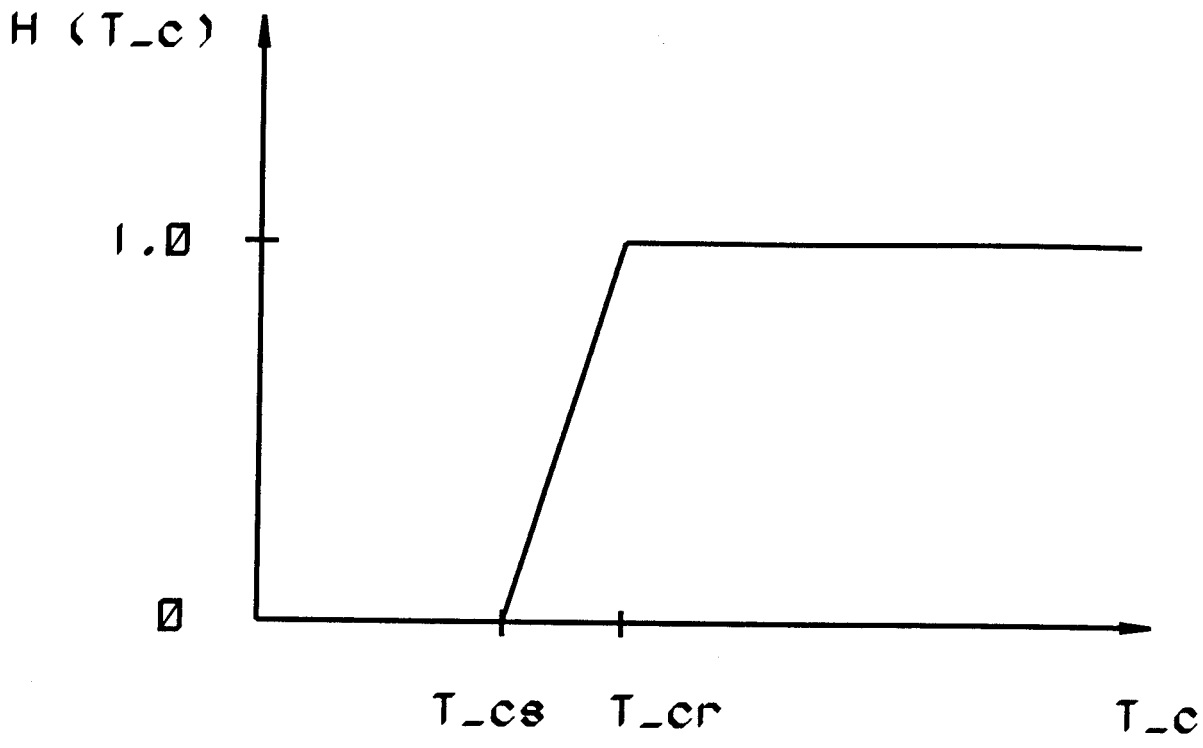

Figure 2: Functional dependence of $H(T_c)$ appearing in Eq. (2).

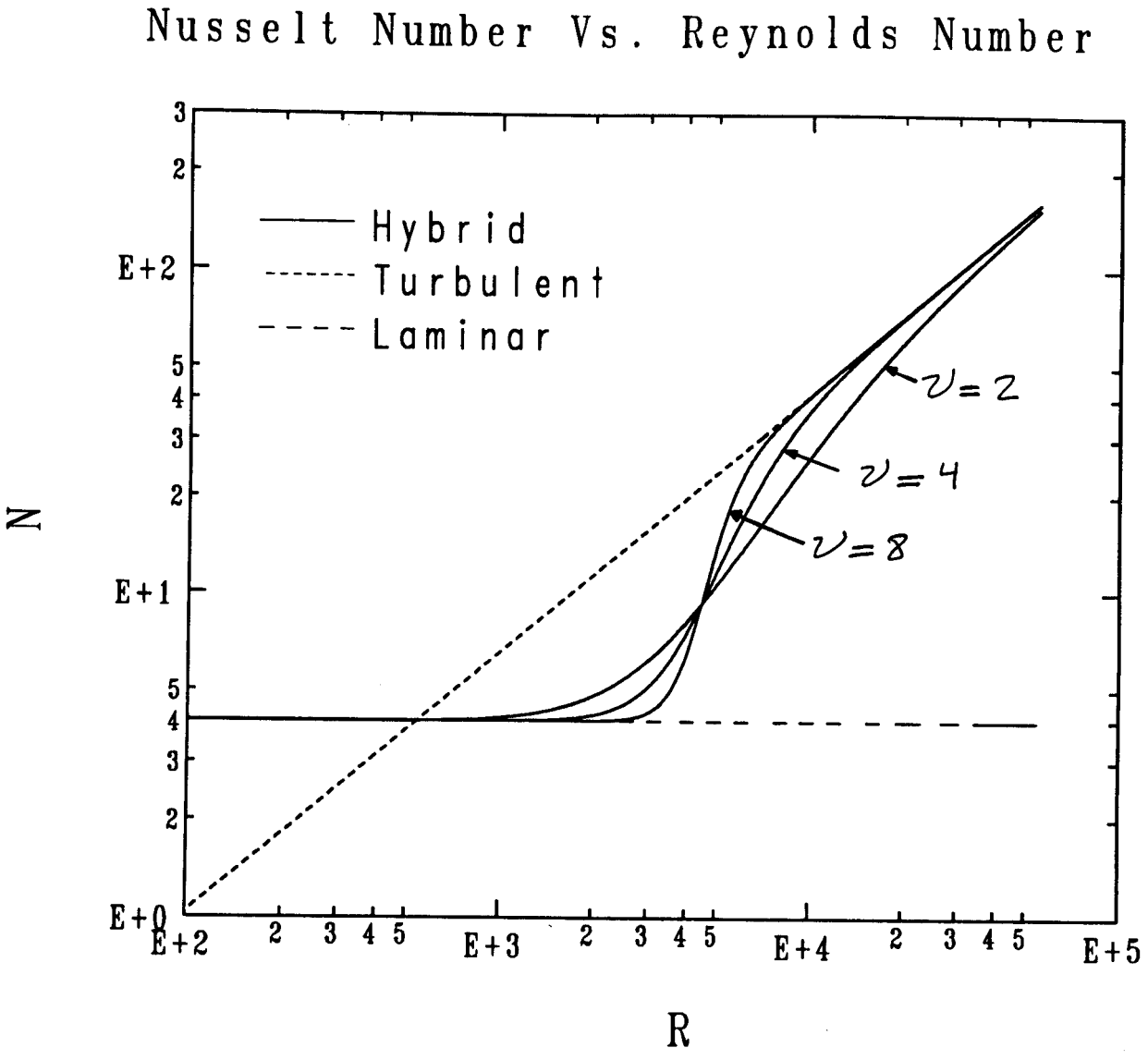

Figure 3: Dependence of Nusselt number on Reynolds number, from Eqs. (28-30).

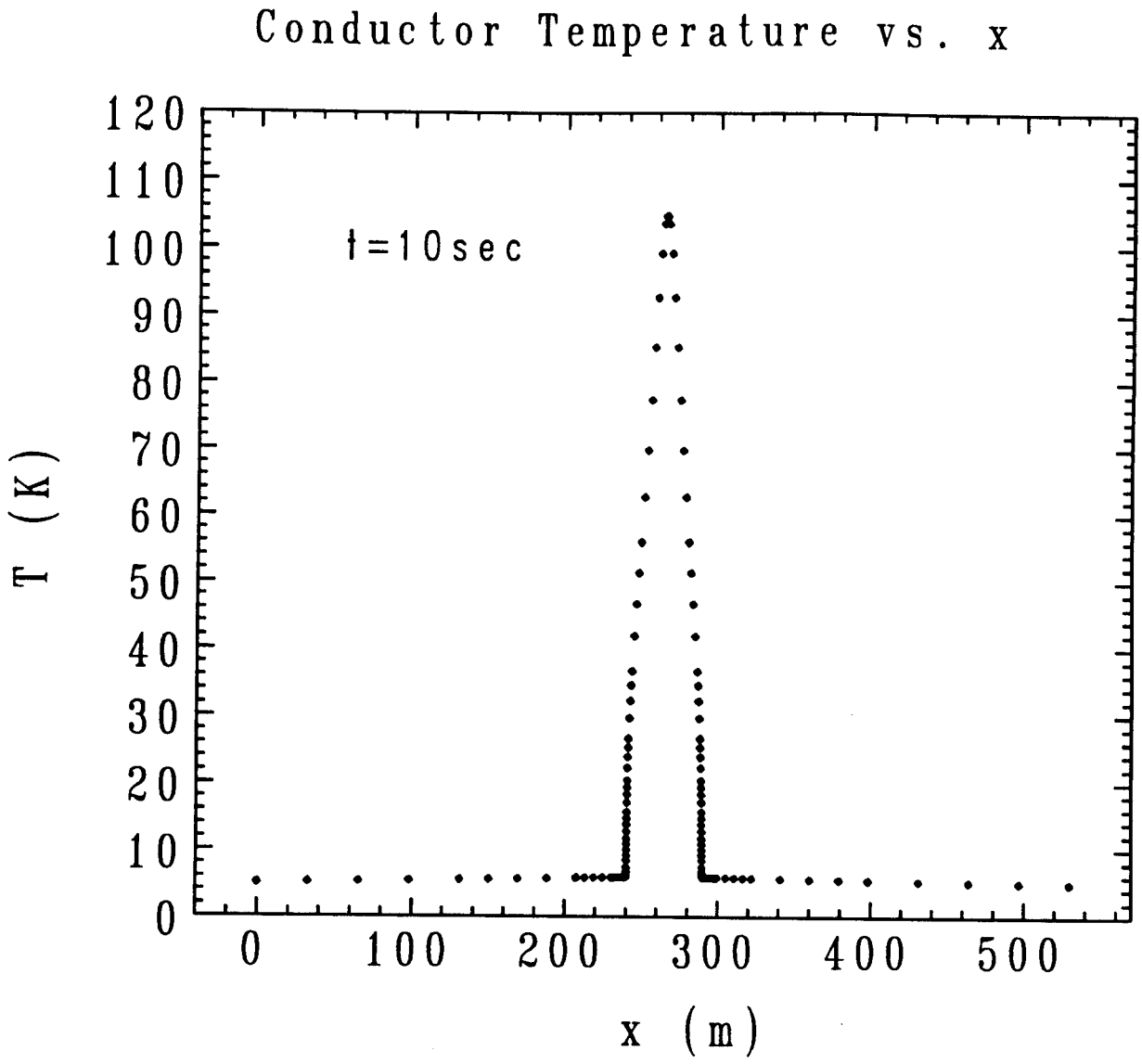

Figure 4a: The conductor/helium temperature profile during quench.

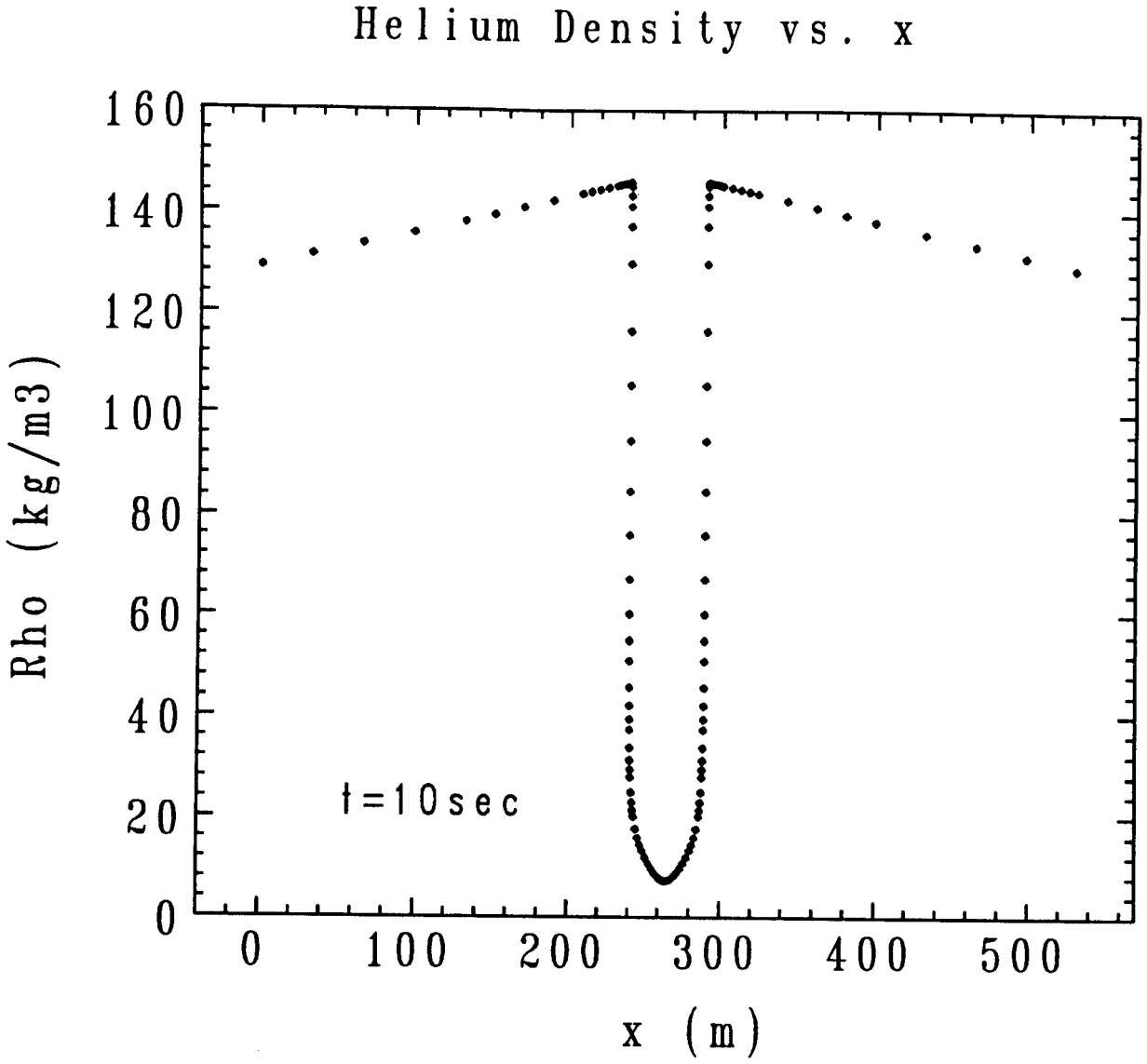

Figure 4b: The helium density profile during quench.

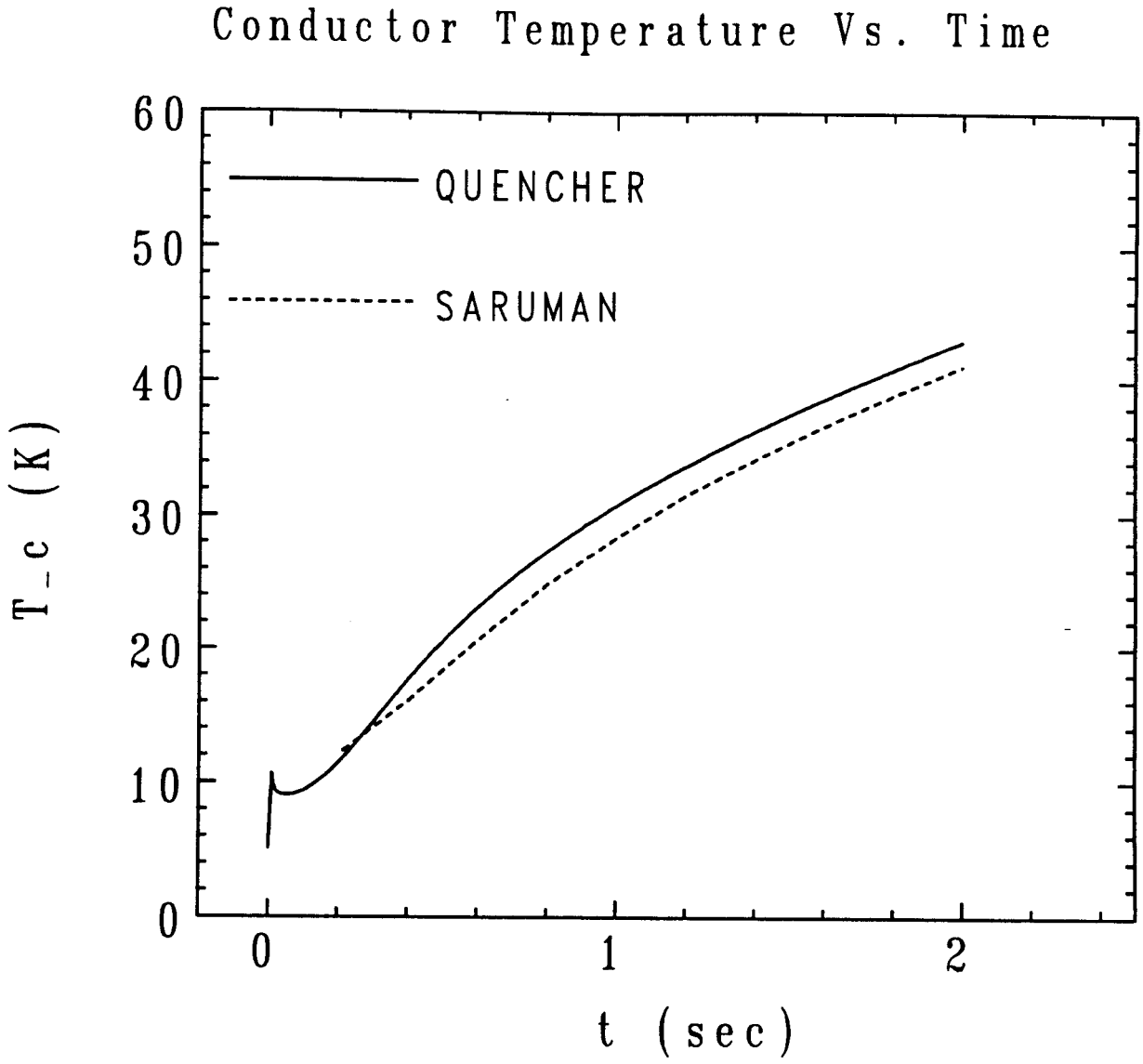

Figure 5a: Comparison of the maximum conductor temperature as calculated by Quencher and Saruman.

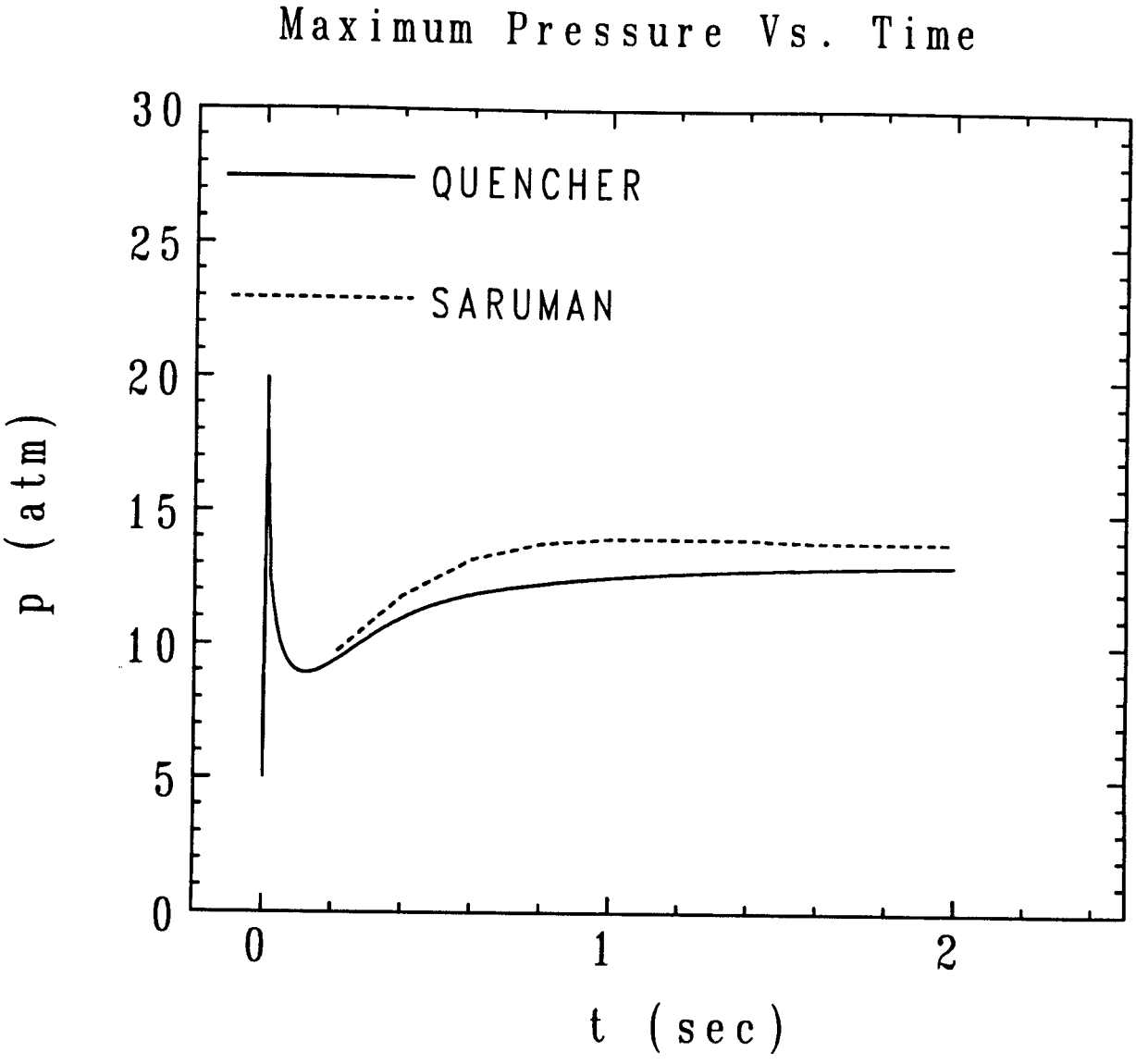

Figure 5b: Comparison of the maximum helium pressure as calculated by Quencher and Saruman.

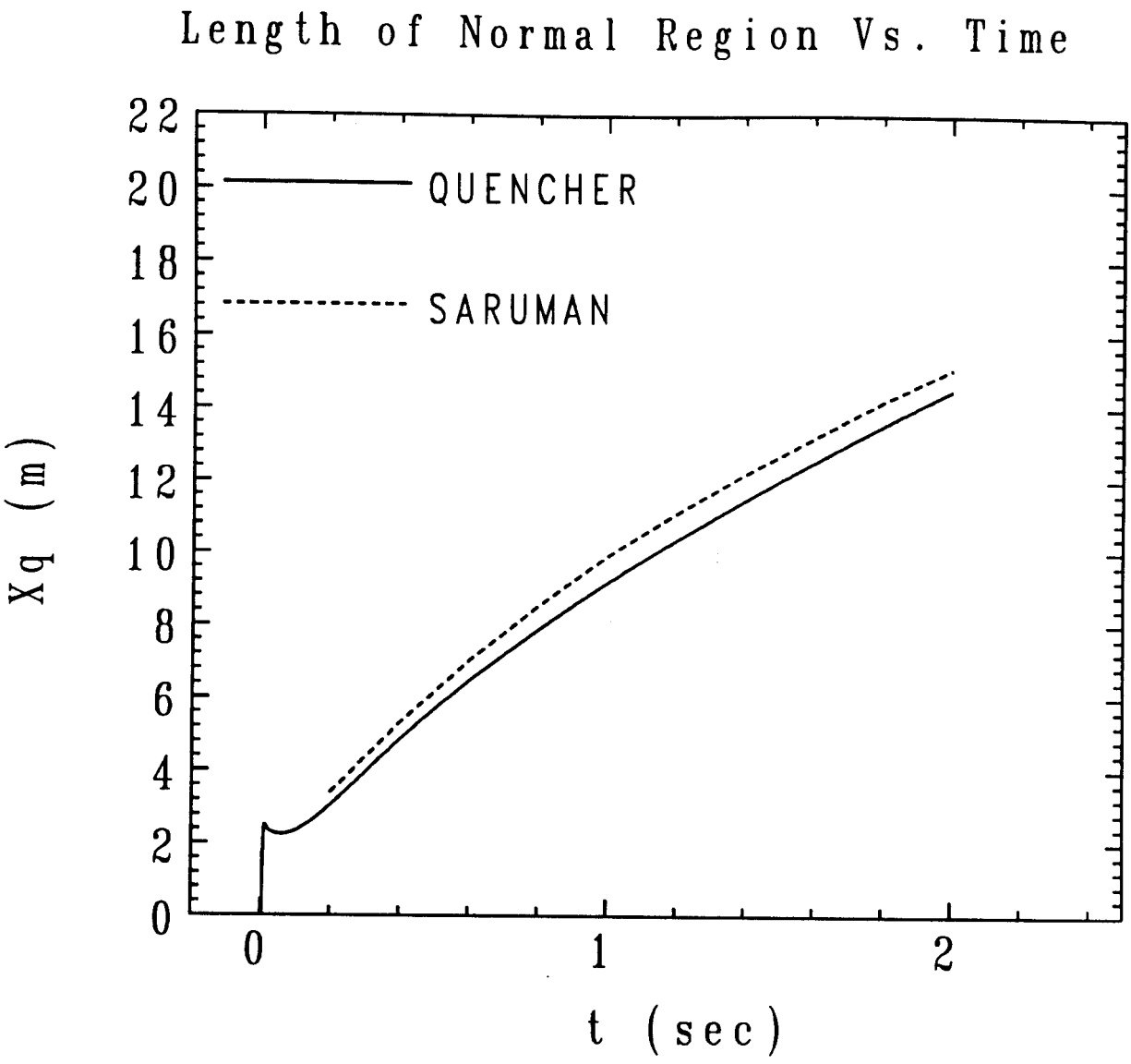

Figure 5c: Comparison of the normal length as calculated by Quencher and Saruman.

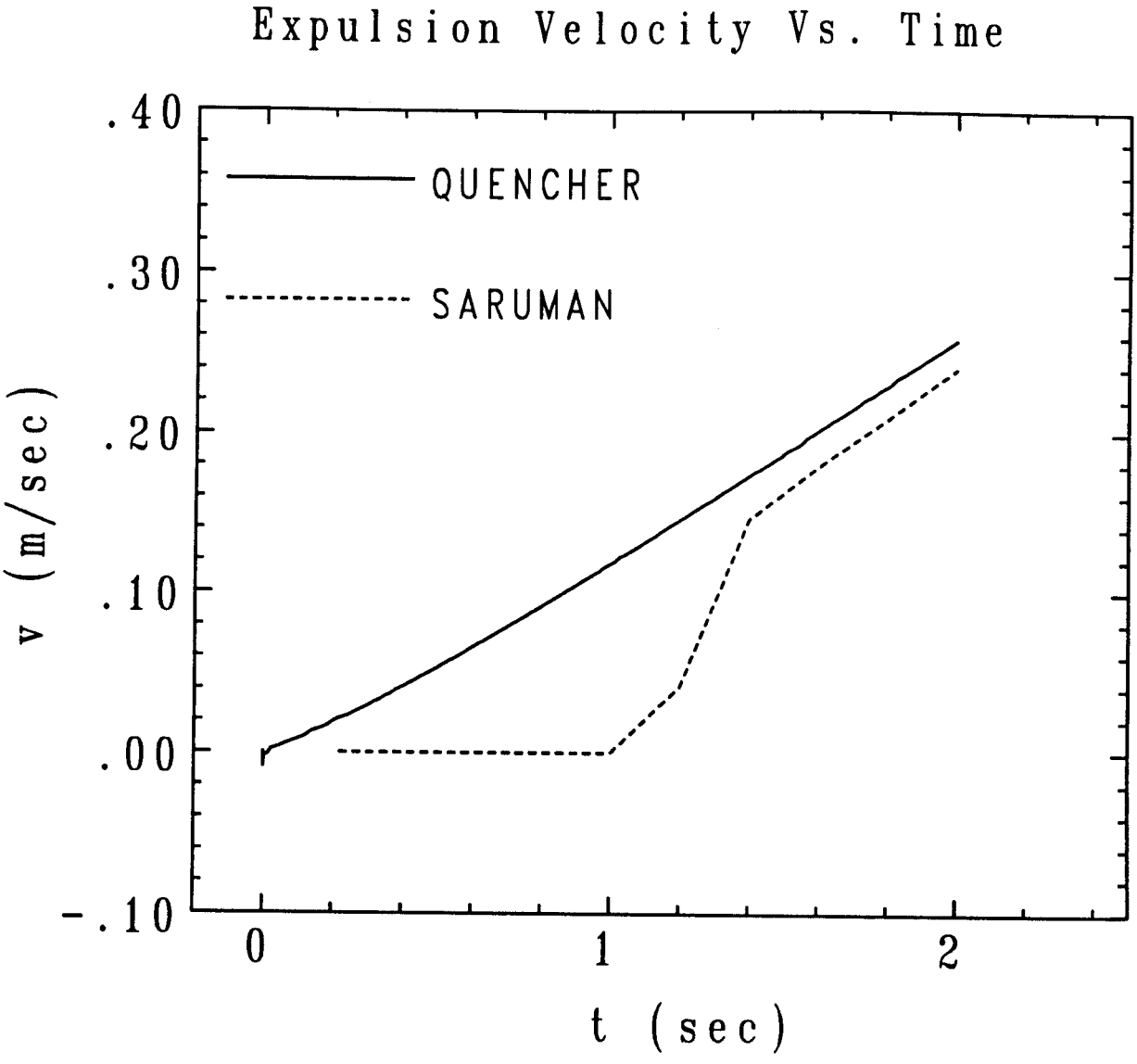

Figure 5d: Comparison of the helium expulsion velocity as calculated by Quencher and Saruman.

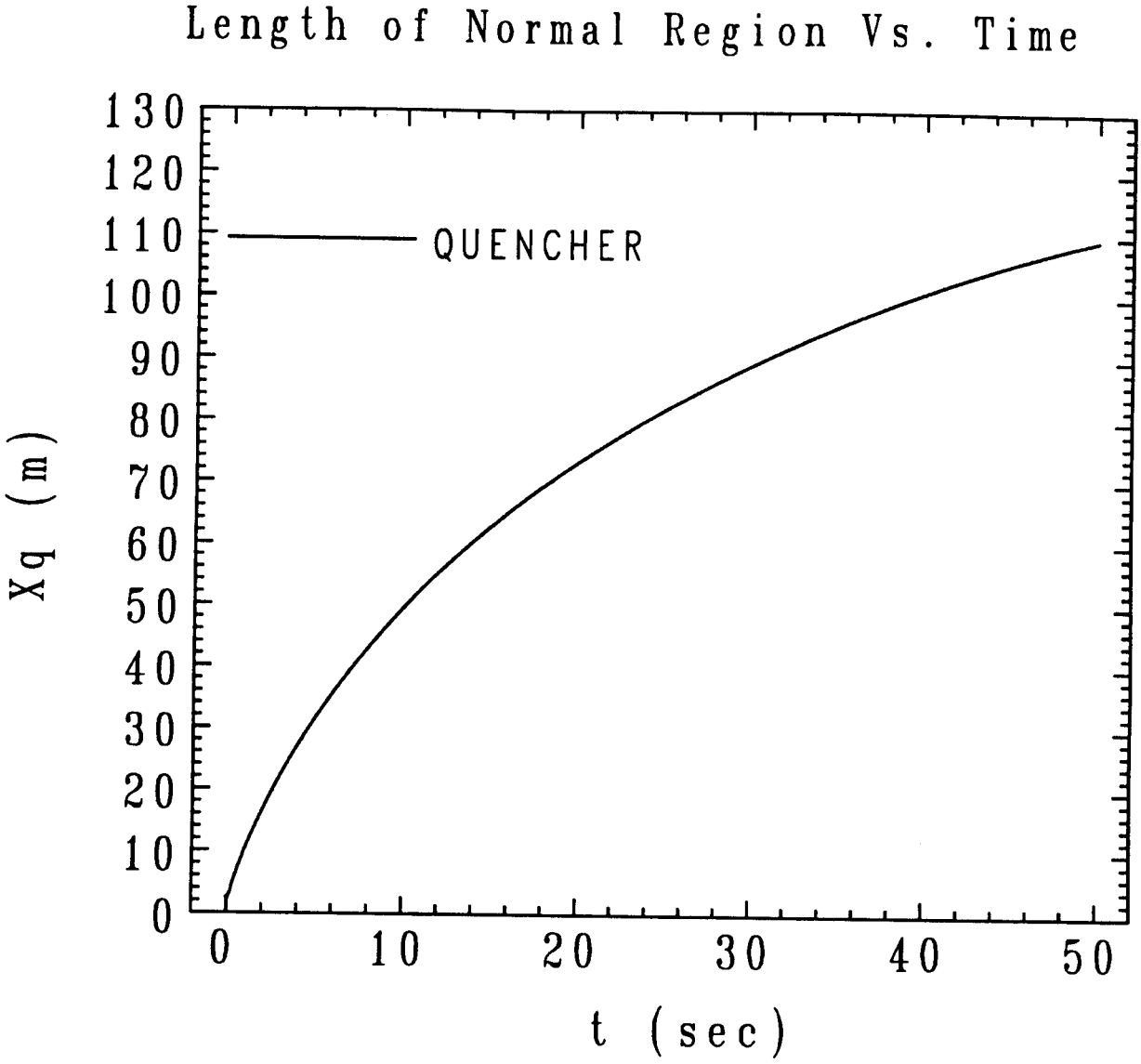

Figure 6: Normal length propagation during a 50 sec quench in the ITER conductor.

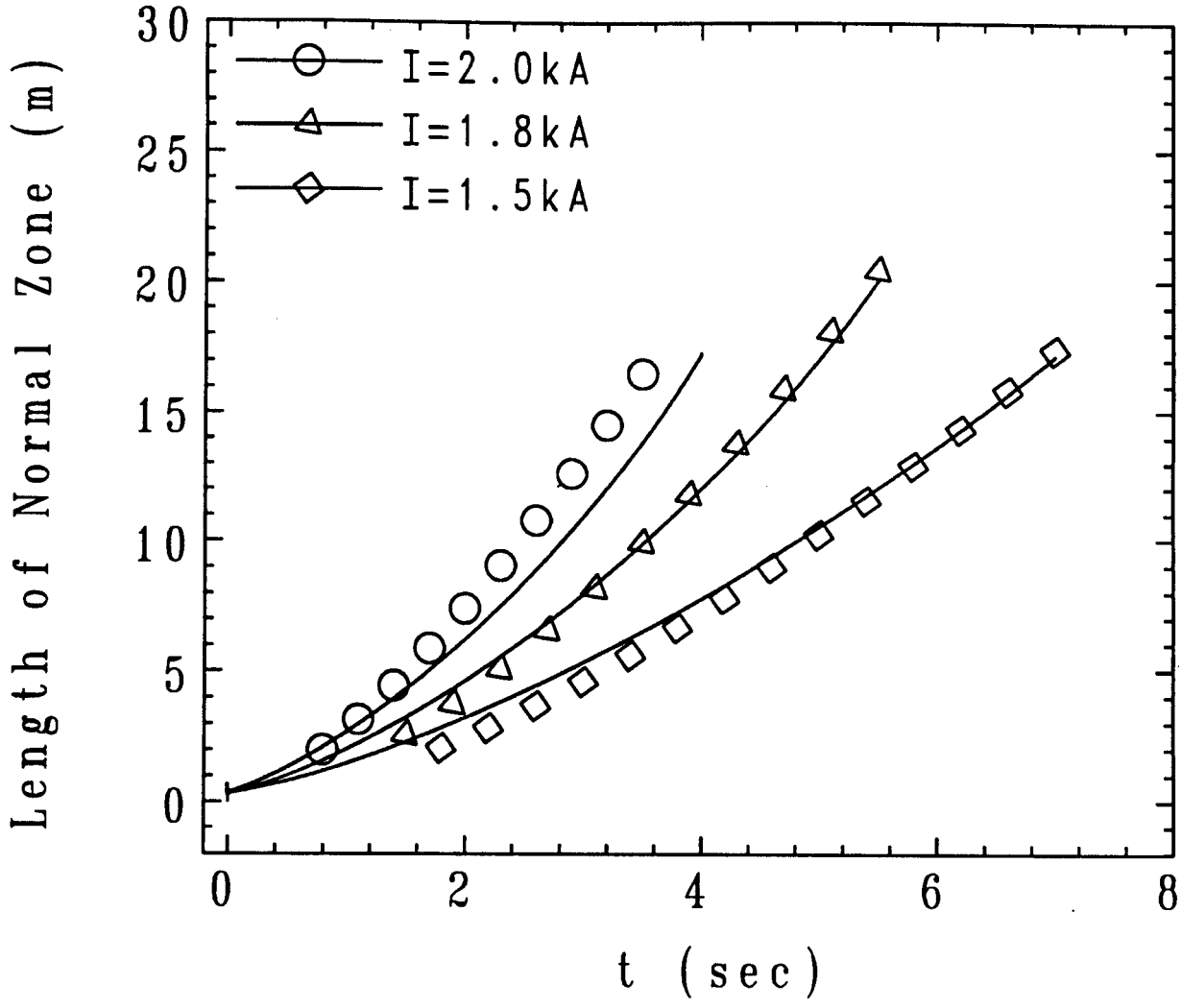

Figure 7: Comparison of Quencher results with experimental data [8].